CO-DIFFUSION FOR P-TYPE PERT SOLAR CELLS USING APCVD BSG LAYERS AS BORON DOPING SOURCE

S. Meier[1], S. Wiesnet[1], S. Mack[1], S. Werner[1] S. Maier[1], S. Unmüßig[1], C. Demberger[2], H. Knauss[2], D. Biro[1], A. Wolf[1]
[1]Fraunhofer Institute for Solar Energy Systems ISE, Heidenhofstraße 2, 79110 Freiburg, Germany
[2]Gebr. SCHMID GmbH, Robert-Bosch-Str. 32-36, 72250 Freudenstadt, Germany
Phone: +49 761 45 88 5059; Fax: + 49 761 45 88 9250; Email: sebastian.meier@ise.fraunhofer.de

ABSTRACT: In this work, we investigate boron-doped back surface field (BSF) formation from borosilicate glass (BSG) deposited by atmospheric pressure chemical vapor deposition (APCVD). Carrier lifetime samples with different boron concentration in the BSG are exposed to high-temperature processes with varying temperature and gas atmospheres. The development aims at producing p-type Si-based passivated emitter and rear totally diffused (PERT) cells in a $POCl_3$ co-diffusion process. Our experiments confirm the critical impact of the O_2 concentration on boron diffusion from APCVD BSG layers. For different peak temperatures Si surface oxidation formation need to be balanced carefully. Moderate diffusion temperatures of 875°C (30 min) yield a BSF doping with R_{sh} = 131 Ω/sq and a recombination current density of $J_{0,BSF}$ = 21 fA/cm² (planar surface, AlO_x/SiN_x-passivation). Finally, 156 mm sized PERT cells fabricated from p-type Czochralski-grown Si wafers using the developed co-diffusion process show peak efficiencies of 20.6%, confirming the feasibility of our co-diffusion approach.
Keywords: APCVD, boron-doping, BSG, PERT, co-diffusion

1 INTRODUCTION

Bifacial passivated emitter and rear (PERC) solar cells allow for conversion efficiencies beyond 21% while enabling bifacial module designs [1]. The bifacial operation allows for increasing the energy yield or a broadening of the energy output over a day, depending on the physical surrounding and module placement [2]. Currently, bifacial PERC cells reach rear efficiencies of 16.7%, where the high shading loss of the rear aluminum grid is a major limitation [1]. One approach to reduce these losses is to use a passivated emitter and rear totally diffused (PERT) cell structure that allows significantly higher rear finger spacing due to additional lateral conductance of the back surface field (BSF). In addition, PERT cells tolerate high resistivity wafers, which reduce light induced degradation (LID) due to boron-oxygen complex recombination [3]. In state of the art processing emitter and BSF of PERT solar cells are formed using sequential diffusion processes with $POCl_3$ and BBr_3 as liquid dopant precursor [4–6]. The additional diffusion step compared to PERC manufacturing implicates additional process complexity and cost. To avoid this additional effort, we present a fast and cost-effective approach to form the phosphorus-doped emitter and boron-doped BSF in one single co-diffusion process. Therefore we investigate co-diffusion from $POCl_3$ atmosphere and a pre deposited borosilicate glass (BSG) layer by atmospheric pressure chemical vapor deposition (APCVD). Main advantage of this approach is its industrial feasibility while keeping the flexibility to independently adjust doping profiles [7].

This paper first discusses the development of a $POCl_3$-based co-diffusion tube furnace process suitable for the fabrication of p-type PERT solar cells. Finally, we prove the co-diffusion concept by fabricating monofacial PERT solar cells from p-type Czochralski-grown silicon (Cz-Si) wafers.

2 APPROACH

2.1 Boron-doping from APCVD BSG layers

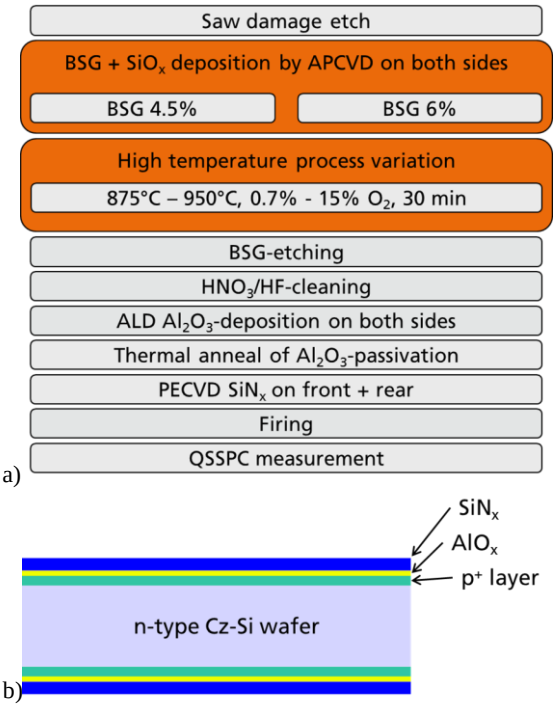

Fig. 1: a) Process sequence and b) sample design for symmetric samples used to characterize boron diffused surfaces made from APCVD BSG layers.

We first investigate boron-doping for BSF formation from APCVD BSG layers with respect to sheet resistance, doping profile and carrier recombination. Fig. 1 represents a) the process scheme and b) the sample design used to develop boron diffusion from APCVD BSG layers.

We use n-type Cz-Si wafers with base resistivity ρ_B = 2.2 Ωcm (determined after thermal processing) and

an edge length of 156 mm for symmetric carrier lifetime samples. Another set of n-type Cz-Si wafers is selected for four point probe (4pp) and electrochemical capacitance voltage (ECV) measurements. All wafers receive a saw damage etch. Then, the deposition of the

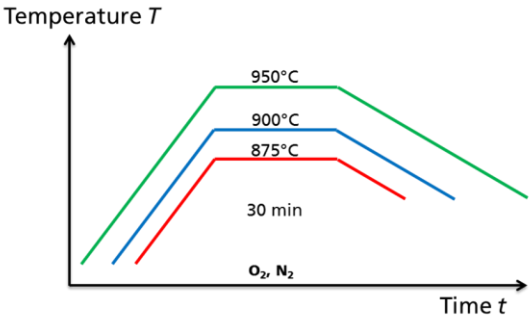

Fig. 2: Schematic of the applied high temperature processes. Peak temperatures T_{Peak} = 875°C, T_{Peak} = 900°C, and T_{Peak} = 950°C are used for a plateau time of 30 minutes. During whole diffusion process the O_2 concentration is kept constant. Different O_2 concentrations from 0% to 3% are investigated.

BSG/SiO_x layer stack in one deposition is realized by APCVD on both sides of the wafer. We apply two different boron-contents of the BSG layer (nominally 4.5% and 6%). Then, diffusion temperatures T_{Peak} = 875°C, T_{Peak} = 900°C, and T_{Peak} = 950°C (all with 30min plateau) at different O_2 concentrations in the atmosphere are applied. Fig. 2 presents a scheme of the high temperature processes.

Following the high temperature step, the BSG/SiO_x layers are removed in HF solution and 4pp and ECV measurements yield sheet resistance R_{sh} and doping profile, respectively. The symmetric carrier lifetime samples receive wet chemical cleaning with a HNO_3/HF sequence, both-sided surface passivation by atomic layer deposition (Fast-ALD) of an Al_2O_3 layer and subsequent out gassing as well as a plasma enhanced chemical vapor deposited (PECVD) SiN_x capping. A fast firing process activates the passivation. Finally quasi steady state photo conductance (QSSPC) measurement determine the dark saturation current $J_{0,BSF}$ using the procedure from Ref. [8].

2.2 Co-diffusion

Based on a high temperature process with T_{Peak} = 875°C, a $POCl_3$-based co-diffusion process is developed. Fig. 3 shows a) the process scheme and b) the sample design.

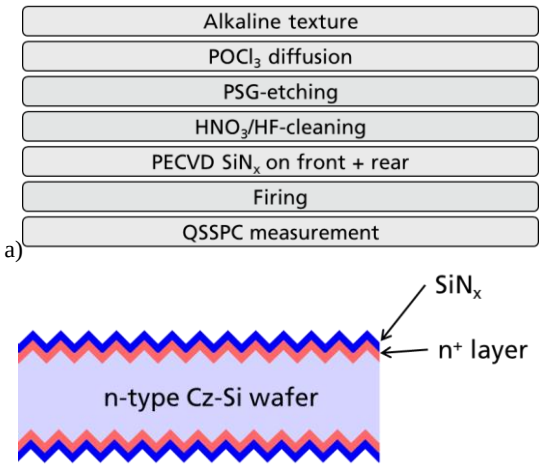

Fig. 3: a) Process sequence and b) sample design used to characterize phosphorus diffused surfaces from $POCl_3$-based co-diffusion process with respect to carrier recombination.

First, n-type Cz-Si wafers with ρ_B = 2.2 Ωcm (determined after thermal processing) and an edge length of 156 mm are alkaline textured. Then, a $POCl_3$-based diffusion with T_{Peak} = 875°C (30min plateau) is applied (see Fig. 4).

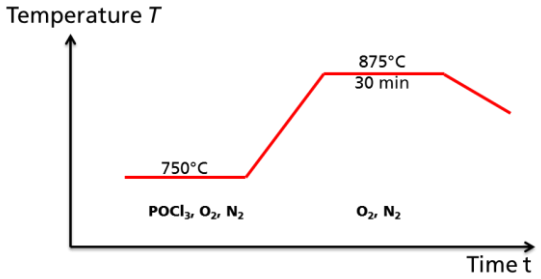

Fig. 4: Schematic of the investigated $POCl_3$-based co-diffusion process.

After phosphosilicate glass (PSG) removal, 4pp and ECV measurements are realized using saw damage etched n-type Si-reference wafers. These wafers are processed in parallel to alkaline textured Si wafers. The textured symmetric n-type Cz-Si lifetime samples receive wet chemical cleaning with a HNO_3/HF sequence, PECVD SiN_x passivation and firing. Finally, QSSPC measurements determine emitter saturation current J_{0e}; see Ref. [8].

2.3 Solar cell fabrication

Fig. 5 represents a process sequence for the fabrication of p-type PERC and co-diffused PERT solar cells.

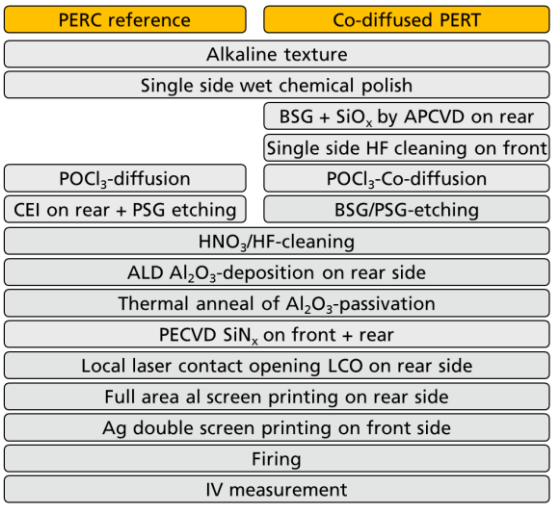

Fig. 5: Process sequence for fabricating PERC (left) and PERT (right) type solar cells.

P-type Cz-Si wafers with an edge length of 156 mm, ρ_B = 2.9 Ωcm and an initial thickness W = 180 µm are textured in an alkaline solution. In a second step the rear side texture is smoothed by a single side wet chemical polish.

For the PERT cells, a BSG/SiO_x layer system is deposited on the polished rear surface by APCVD in one single process, followed by a single side HF cleaning sequence for the non-deposited front side. The wafers are then subjected to a $POCl_3$-based co-diffusion tube furnace process to simultaneously form a phosphorus doped emitter on the front side and a boron doped BSF on the rear side of the PERT cell. An HF bath then removes the formed PSG and BSG layers.

In contrast, the PERC reference cells are directly subjected to a standard $POCl_3$-diffusion process [9]. The rear side of PERC cell is then subjected to wet chemical edge isolation (CEI) followed by front PSG removal.

PERC and PERT cells thus differ in diffusion sequence; however, after diffusion their fabrication is similar. Rear passivation is realized by an Al_2O_3 layer deposited by Fast-ALD followed by thermal anneal of the Al_2O_3 layer. Then a SiN_x layer is deposited on top of the Al_2O_3 layer. The phosphorus doped emitter at the front side is passivated by a SiN_x layer deposited by PECVD. Then, local contact opening (LCO) of line shaped rear contacts is realized by a laser process and a full-area aluminum paste is applied by screen-printing. Note that for both PERC and PERT cells an identical line pitch of 700 µm is chosen (optimized for the PERC structure). The emitter side is subjected to a double screen printing step using a commercially available silver paste. Final steps are contact formation by a firing step in a commercial fast firing oven (variation of peak temperature) and IV measurement using an industrial cell tester.

3 RESULTS

3.1 Influence of peak temperature on boron concentration

Fig. 6 presents boron doping profiles for BSG layers with 6% boron concentration from diffusions with T_{Peak} = 875°C, T_{Peak} = 900°C, and T_{Peak} = 950°C, all with an O_2 concentration of 0.7% in the diffusion atmosphere (see Fig. 2 for the schematic of the high-temperature processes). The used samples are fabricated as described in section 2.1, see Fig. 1 and Fig. 2.

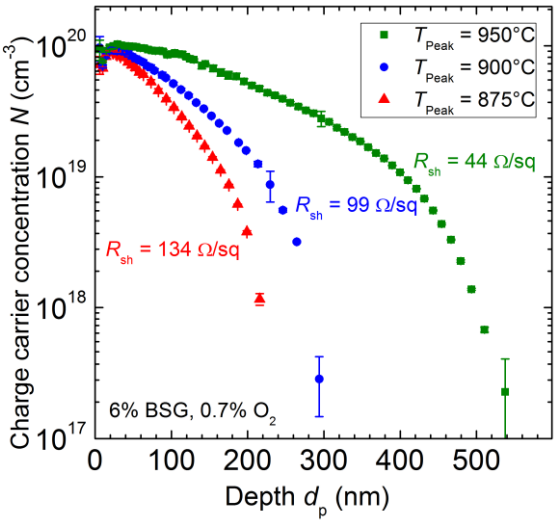

Fig. 6: Boron doping profiles measured by ECV (wafer center) on SDE surfaces for BSG layers with 6% concentration and diffusion processes with different peak temperatures T_{Peak}, all with an O_2 concentration of 0.7% in the diffusion atmosphere. The measured sheet resistances R_{sh} (center, 4pp) are given as well.

With increasing temperature, the profile depth d_P increases from $d_P \approx 240$ nm at T_{Peak} = 875°C to $d_P \approx 540$ nm at T_{Peak} = 950°C. The maximum carrier concentration N_{max} for the diffusions with T_{Peak} = 875°C and T_{Peak} = 900°C is $N_{max} \approx 9\times10^{19}$ cm^{-3} and increases slightly to $N_{max} \approx 1\times10^{20}$ cm^{-3} for T_{Peak} = 950°C. Accordingly, the sheet resistance R_{sh} reduces from R_{sh} = 134 Ω/sq. at T_{Peak} = 875°C to R_{sh} = 44 Ω/sq. at T_{Peak} = 950°C. All profiles show a slightly depleted surface concentration due to segregation of boron into the oxide surface layer [10,11].

3.2 Influence of O_2 concentration on boron concentration

The impact of the O_2 concentration during the thermal process on boron diffusion from APCVD BSG layers is discussed for T_{Peak} = 875°C. Doping profiles resulting after these diffusion processes are shown in Fig. 7, see Fig. 1 and Fig. 2.

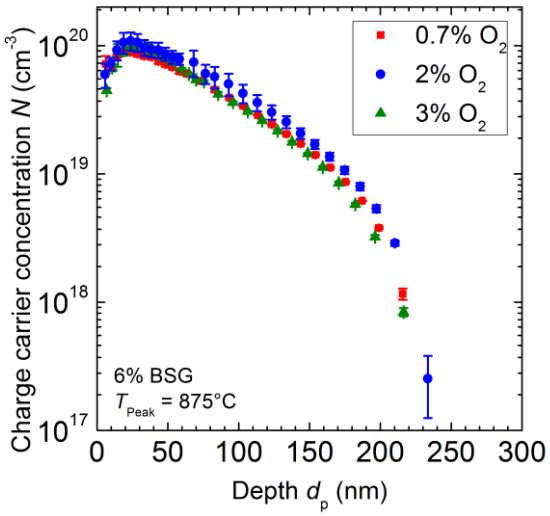

Fig. 7: Boron doping profiles measured by ECV (wafer center) on SDE surfaces for BSG layers with 4,5% and 6% concentration and high-temperature processes with T_{Peak} = 875°C and different O_2 concentrations in the process atmosphere.

All measured doping profiles show a high agreement. The boron doping is characterized by $N_{max} \approx 9\times10^{19}$ cm^{-3} and $d_P \approx 240$ nm. However, the highest oxygen concentration of 3% shows the strongest surface depletion, which is reasonable, since high oxygen concentrations enhance the oxide growth and boron segregation into the oxide [11,10].

The R_{sh} measurements by 4pp (see Table I) reveal slight differences of the processes.

Table I: Sheet resistance measurements (4pp) of the boron-doping on 156mm n-type wafers with 400 measurement points per wafer by 4pp. The given data is organized in R_{sh} on the center of the Si wafer, average R_{sh} over the wafer surface and standard deviation.

sample	R_{sh} center [Ω/sq]	R_{sh} average [Ω/sq]	R_{sh} std. dev. [Ω/sq]
4.5% BSG 0.7% O_2	128	142	41
6% BSG 0.7% O_2	134	131	11
6% BSG 2% O_2	114	116	9
6% BSG 3% O_2	135	163	71

For the process with 0.7% O_2 content, increasing the boron concentration from 4.5% to 6% reduces the average R_{sh} = (131 ± 41) Ω/sq to R_{sh} = (131 ± 11) Ω/sq and increases the homogeneity of R_{sh}. If the O_2 concentration is increased to 2% and higher, no boron diffusion can be observed for a BSG layer with 4.5%. In contrast, for a BSG layer with 6% content, R_{sh} slightly reduces from R_{sh} = (131 ± 11) Ω/sq to R_{sh} = (116 ± 9) Ω/sq, whereas a further increase from 2% to 3% O_2 concentration again increases R_{sh} = (163±71) Ω/sq. The inhomogeneous distribution of R_{sh} is observed on the border of the Si wafer.

In conclusion, high O_2 concentrations tend to increase the sheet resistance. Additionally the non-uniformity of the sheet resistance over the Si-wafer is increased if the O_2 concentration is increased. We attribute these effects to a thermally grown SiO_2 layer at the interface Si-wafer to BSG layer. This SiO_2 layer acts as diffusion barrier against boron from BSG layer and even leads to complete decoupling of the BSG layer for higher oxygen concentrations.

3.3 Dark saturation current densities for diffusion processes with peak temperature of 875°C.

Dark saturation current densities $J_{0,BSF}$ for boron BSF diffusion processes with T_{Peak} = 875°C (section 2.1 Fig. 2 and Fig. 3) are shown in Fig.8.

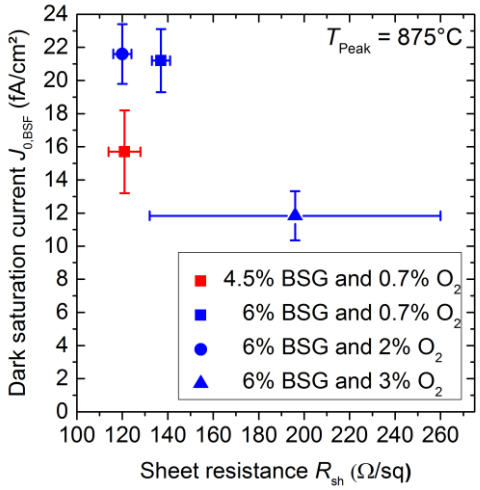

Fig. 8: Dark saturation current density $J_{0,BSF}$ (planar surface, AlO_x/SiN_x-passivation, average and standard deviation of five measurement points per wafer) over average value of sheet resistance R_{sh} (average R_{sh} measured by means of inductive coupling using an inline tool [12]) for diffusion processes at T_{Peak} = 875°C.

The observed recombination currents are very low and range from $J_{0,BSF}$ = (22 ± 2) fA/cm^2 at R_{sh} = (121 ± 7) Ω/sq to $J_{0,BSF}$ = (12 ± 1) fA/cm^2 for R_{sh} = (196 ± 64) Ω/sq. The graph shows average R_{sh} measured by means of inductive coupling using an inline tool [12].

With respect to a homogeneous distribution of the sheet resistance 4.5% boron concentration and 0.7% O_2 concentration as well as 6% boron concentration and 3% O_2 concentration are not well suited for the fabrication of PERT cells. Thus, for the fabrication of co-diffused PERT cells 6% boron content and a diffusion process with an O_2 concentration of 0.7% are selected.

3.3 Characterization of full co-diffusion process

Based on 6% boron concentration in the BSG layer and 0.7% O_2 content in the diffusion atmosphere the final co-diffusion process shown in Fig. 4 is developed. The resulting doping profiles measured by ECV are shown in Fig. 9.

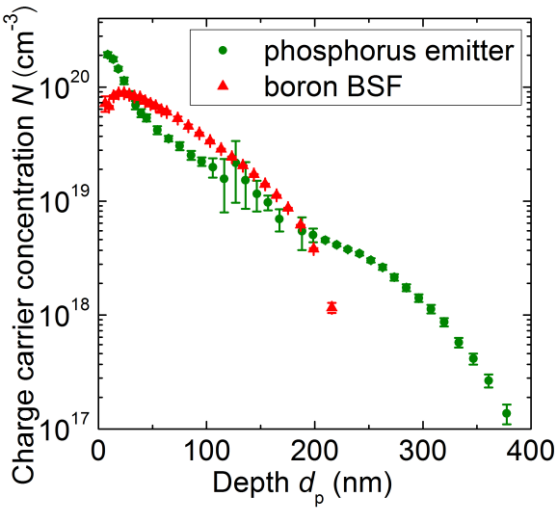

Fig. 9: ECV measurement of the co-diffusion process for simultaneous boron diffusion (red symbols) from an APCVD BSG/SiO_x-layer stack and phosphorus diffusion (green symbols) from a $POCl_3$ ambient.

The samples are processed as described in section 2.1 Fig. 3. The Phosphorus doped emitter is characterized by $N_{max} \approx 2\times10^{20}$ cm^{-3} and $d_P \approx 380$nm. This results in $R_{sh} = (90 \pm 2)$ Ω/sq. measured by means of inductive coupling using an inline tool [12] and $J_{0e} = (79 \pm 15)$ fA/cm^2 for an alkaline textured and passivated (SiN_x) surface.

3.3 Comparison PERC and co-diffused PERT solar cells

Based on the developed co-diffusion process (Fig. 4) monofacial PERT cells are fabricated and compared to monofacial PERC cells based on standard $POCl_3$ diffusion process developed at Fraunhofer ISE [9]. Fig. 10 illustrates the different cell structures which are fabricated according to the process plan in Fig. 5.

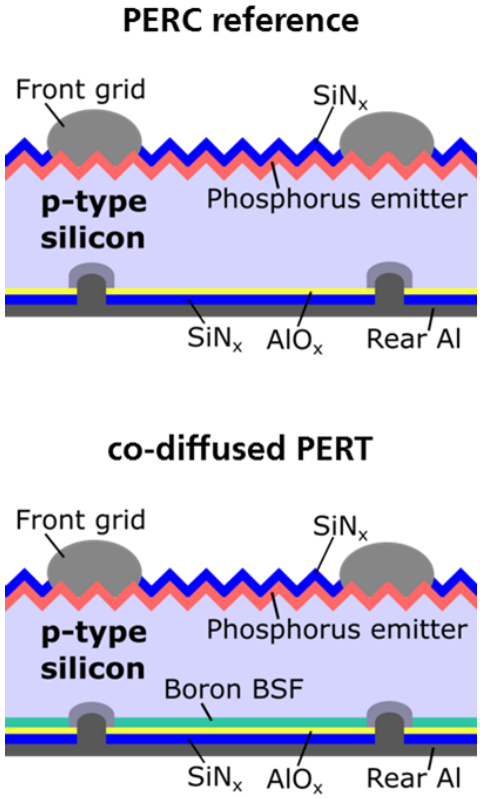

Fig. 10: Investigated PERC and PERT cell structures fabricated according to the process plan in Fig. 5. PERT cells are fabricated with a $POCl_3$-based co-diffusion process (see Fig. 4). For the PERC cells a standard $POCl_3$ based diffusion process is used [9].

The results of IV measurements using an industrial cell tester for the different cell types are presented in Table II.

Table II: IV data (as processed) for PERC and PERT solar cells with an edge length of 156 mm and $\rho_B = 2.9$ Ωcm using an industrial cell tester. Shown are the median values of best peak firing temperature groups.

Cell type	V_{oc} [mV]	J_{sc} [mA/cm^2]	FF [%]	η [%]	R_p [kΩcm^2]	R_s [Ωcm^2]
PERC reference	653	39.6	79.3	20.5	109	0.5
PERT co-diff.	649	39.4	80.3	20.5	52	0.4

Median values of best groups of PERC and PERT cells are shown. The PERC reference cells show 4 mV higher V_{oc} and 0.2 mA/cm² higher J_{sc}. This is attributed to an increased rear surface recombination of the PERT cells. Control samples of this batch showed an increased $J_{0,BSF} = (152 \pm 35)$ fA/cm^2, much higher than observed in previous runs (see Fig. 8). The lateral conductance of the BSF increases the FF of the PERT cells by 1%$_{abs}$ to $FF = 80.3\%$. Thus, both cell types show the same efficiency level of $\eta = 20.5\%$. Peak efficiencies are 20.7% for PERC and 20.6% for PERT.

4 SUMMARY AND CONCLUSION

We investigate boron doping from APCVD BSG/SiO_x layer stacks. At moderate diffusion conditions of 875°C for 30 min, average sheet resistances of R_{sh} = 116 to 163 Ω/sq are observed with low recombination parameters of $J_{0,BSF}$ = 22 to 12 fA/cm^{2,} respectively (planar surface Al_2O_3/SiN_x passivation). With these conditions, we develop a $POCl_3$-based co-diffusion process leading to a simultaneous phosphorus-diffusion of R_{sh} = (90 ± 2) Ω/sq. measured by inline-R_{sh} measurement and J_{0e} = (79 ± 15) fA/cm^2. Finally, we prove the co-diffusion concept by fabricating monofacial PERT solar cells with peak efficiencies of 20.6% and 20.5% (median value) on 156mm 2.9 Ωcm p-type Cz-substrates.

In conclusion, co-diffusion using APCVD BSG layers and $POCl_3$-diffusion is a promising approach for PERT cell fabrication, enabling high quality boron BSF formation with excellent recombination properties. Relevant applications are bifacial PERT cells with increased rear efficiency due to reduced shading as well as minimization of LID due to high tolerance of PERT cells to high resistivity wafers.

5 ACKNOWLEDGEMENTS

The authors thank development team of APCVD of Gebr. SCHMID GmbH and all colleagues at the Fraunhofer ISE Photovoltaic Technology Evaluation center (PV-TEC).

The authors would like to thank TOYO for the provision of aluminum pastes for the rear side of PERC and PERT solar cells.

S. Meier gratefully acknowledges the scholarship of the “Heinrich Böll Stiftung“.

This work was funded by the German Federal Ministry for Economic Affairs and Energy within the research project “KoKoBi“ under contract 0325875B.

6 REFERENCES

[1] T. Dullweber, C. Kranz, R. Peibst et al., "PERC+: industrial PERC solar cells with rear Al grid enabling bifaciality and reduced Al paste consumption", *Prog. Photovolt: Res. Appl.*, pp. n/a-n/a, 2015.

[2] T. S. Böscke, D. Kania, A. Helbig et al., "Bifacial n-Type Cells With >20% Front-Side Efficiency for Industrial Production", *IEEE J. Photovoltaics*, vol. 3, no. 2, pp. 674–677, 2013.

[3] K. Bothe, R. Sinton, J. Schmidt, "Fundamental boron-oxygen-related carrier lifetime limit in mono- and multicrystalline silicon", *Progress in Photovoltaics: Research and Applications*, vol. 13, pp. 287–296, 2005.

[4] A. Teppe, C. Gong, K. Zhao et al., "Progress in the industrial evaluation of the mc-Si PERCT technology based on boron diffusion, Constance, 2015.

[5] B. Lim, F. Kiefer, N. Wehmeier et al., "Simplifying the fabrication of n-PERT solar cells: Recent progress at ISFH", *Photovoltaics International*, 2015.

[6] B. Lim, F. Kiefer, T. Brendemühl et al., "Bifacial n-PERT solar cells with 20.4% efficiency applying dual print, Hertogenbosch, 2014.

[7] P. Rothhardt, S. Meier, K. Jiang et al., "19.9 % efficient bifacial n-type solar cell produced by co-diffusion-cobin, Amsterdam, 2014, pp. 653–655.

[8] A. Kimmerle, J. Greulich, A. Wolf, "Carrier-diffusion corrected J0-analysis of charge carrier lifetime measurements for increased consistency", *Solar Energy Materials and Solar Cells*, vol. 142, pp. 116–122, 2015.

[9] S. Werner, E. Lohmüller, S. Maier et al., "Process Optimization for the Front Side of p-Type Silicon Solar Cells, Amsterdam, The Netherlands, 2014.

[10] K. Taniguchi, K. Kurosawa, M. Kashiwagi, "Oxidation Enhanced Diffusion of Boron and Phosphorus in (100) Silicon", *J. Electrochem. Soc.: Solid-state Science and Technology*, vol. 127, no. 10, p. 6, 1980.

[11] A. S. Grove, O. Leistiko, C. T. Sah, "Redistribution of acceptor and donor impurities during thermal oxidation of silicon", *J. Appl. Phys.*, vol. 35, no. 9, p. 2695, 1964.

[12] M. Spitz, U. Belledin, S. Rein, "Fast inductive inline measurement of the emitter sheet resistance in industrial solar cell fabrication, Milano, 2007, pp. 47–50.